Galectin-1 deficiency improves axonal swelling of motor neurones in SOD1G93A transgenic mice

小早川, 優子

https://doi.org/10.15017/1441123

出版情報：九州大学, 2013, 博士（医学）, 課程博士
バージョン：

Galectin-1 deficiency improves axonal swelling of motor neurons in SOD1^{G93A} transgenic mice

Yuko Kobayakawa[a,b], Kunihiko Sakumi[a,c], Kosuke Kajitani[a,d], Toshihiko Kadoya[e], Hidenori Horie[f], Jun-ichi Kira[b], Yusaku Nakabeppu[a,c]

[a]Division of Neurofunctional Genomics, Department of Immunobiology and Neuroscience, Medical Institute of Bioregulation, Kyushu University, Fukuoka 812-8582, Japan

[b]Department of Neurology, Neurological Institute, Graduate School of Medical Sciences, Kyushu University, Fukuoka 812-8582, Japan

[c]Research Center for Nucleotide Pool, Kyushu University, Fukuoka 812-8582, Japan

[d]Department of Neuropsychiatry, Graduate School of Medical Sciences, Kyushu University, Fukuoka 812-8582, Japan

[e]Department of Biotechnology, Maebashi Institute of Technology, Maebashi 371-0816, Japan

[f]TechnoMaster Co. Ltd., Yokohama 236-0038, Japan

Corresponding author: Dr. Yusaku Nakabeppu, Division of Neurofunctional Genomics, Department of Immunobiology and Neuroscience, Medical Institute of Bioregulation, Kyushu University, 3-1-1 Maidashi Higashi-ku, Fukuoka 812-8582, Japan. Tel: +81-92-642-6800. E-mail: yusaku@bioreg.kyushu-u.ac.jp

Keywords: galectin-1, SOD1, amyotrophic lateral sclerosis, axonal spheroid, axonal degeneration

Short running title: Galectin-1 is associated with axonal degeneration in SOD1^{G93A} mice

Abstract

Aims: Galectin-1, a member of the β-galactoside-binding lectin family, accumulates in neurofilamentous lesions in the spinal cords of both sporadic and familial amyotrophic lateral sclerosis (ALS) patients with a superoxide dismutase 1 gene (*SOD1*) mutation (A4V). The aim of this study was to evaluate the roles of endogenous galectin-1 in the pathogenesis of ALS. **Methods:** Expression of galectin-1 in the spinal cord of mutant SOD1 transgenic ($SOD1^{G93A}$) mice was examined by pathological analysis, real-time RT-PCR, and western blotting. The effects of galectin-1 deficiency were evaluated by cross-breeding $SOD1^{G93A}$ mice with galectin-1 null ($Lgals1^{-/-}$) mice. **Results:** Before ALS-like symptoms developed in $SOD1^{G93A}/Lgals1^{+/+}$ mice, strong galectin-1 immunoreactivity was observed in swollen motor axons and colocalized with aggregated neurofilaments. Electron microscopic observations revealed that the diameters of swollen motor axons in the spinal cord were significantly smaller in $SOD1^{G93A}/Lgals1^{-/-}$ mice, and there was less accumulation of vacuoles compared with $SOD1^{G93A}/Lgals1^{+/+}$ mice. In symptomatic $SOD1^{G93A}/Lgals1^{+/+}$ mice, astrocytes surrounding motor axons expressed a high level of galectin-1. **Conclusions:** Galectin-1 accumulates in neurofilamentous lesions in $SOD1^{G93A}$ mice, as previously reported in humans with ALS. Galectin-1 accumulation in motor axons occurs before the development of ALS-like symptoms and is associated with early processes of axonal degeneration in $SOD1^{G93A}$ mice. In contrast, galectin-1 expressed in astrocytes may be involved in axonal degeneration during symptom presentation.

Introduction

Amyotrophic lateral sclerosis (ALS) is a fatal disease that produces progressive muscle weakness associated with degeneration of motor neurons. While the majority of ALS patients are sporadic, more than 5% of all cases run in families, with a range from 2 to 15% in different populations [1]. In both sporadic and familial ALS, the presence of axonal spheroids and perikaryal accumulations/aggregations comprised of neuronal intermediate filament proteins, such as neurofilaments and peripherin, is a hallmark pathological feature [2-4]. However, it is largely unknown how these abnormalities occur and what precise contributions they make to the pathogenesis of ALS.

Galectin-1, a member of the β-galactoside-binding lectins, is another component that accumulates in axonal spheroids, cord-like neurite swellings, and conglomerate inclusions of degenerating motor neurons in both sporadic and familial ALS patients, the latter carrying the A4V mutation of the superoxide dismutase 1 gene (*SOD1*) [5]. Galectin family proteins are defined by their affinity for β-galactoside sugars and shared amino acid sequence, which encodes a carbohydrate-recognition domain (CRD) [6]. Galectin-1 is a 14.5-kDa protein with a single CRD in its molecule that allows it to exert carbohydrate-binding activity, which is expressed in various tissues and forms a homodimer in reduction conditions. The reduced form of galectin-1 is known to have multiple functions, such as cell adhesion, migration, and proliferation [7, 8], tumor growth and metastasis [9], apoptosis of activated T cell [10], and interactions with mRNA splicing mechanisms [11]. Particularly in the mouse nervous system, galectin-1 is involved in the formation of the neural networks of the olfactory bulb [12], proliferation of neural stem cells [13, 14], and neurogenesis in the hippocampus [15,

16]. On the other hand, the oxidized form of galectin-1 exists as a monomer and lacks carbohydrate-binding activity [17, 18]. Oxidized galectin-1 has been shown to promote axonal regeneration after axotomy of peripheral nerves [18, 19].

It has been reported that expression of galectin-1 protein is increased in the spinal cord of symptomatic mutant SOD1 transgenic mice [20]. Additionally, administration of the oxidized form of recombinant human galectin-1 to mutant SOD1 transgenic mice delayed the onset of their disease and prolonged the lives of the mice and the duration of their illness, thus demonstrating its neuroprotective role in ALS-model mice [21]. However, it has not yet been elucidated whether endogenous galectin-1 accumulates in degenerating motor neurons of ALS-model mice or whether it has any role in the pathogenesis of ALS.

In the present study, we examined the expression of galectin-1 in the spinal cord of mutant SOD1 transgenic ($SOD1^{G93A}$) mice, and evaluated the roles of galectin-1 by cross-breeding $SOD1^{G93A}$ mice with galectin-1 null (*Lgals1*$^{-/-}$) mice. Our results demonstrate that galectin-1 is associated with the process of axonal degeneration in $SOD1^{G93A}$ mice.

Materials and Methods

Animals

Transgenic mice for the human SOD1^{G93A} gene [B6.Cg-Tg(SOD1*G93A)^{dl}1Gur/J; Stock Number: 002299] were purchased from the Jackson Laboratory (Bar Harbor, ME, USA). They were crossed with C57BL/6J mice (Clea Japan, Tokyo, Japan) to maintain the strains, and hemizygous animals were examined in the experiments. The copy number of the transgene was confirmed using quantitative polymerase chain reaction (qPCR) assay according to a previously described method [22]. Galectin-1 knockout mice (*Lgals1*$^{-/-}$) were established as previously described [23] and backcrossed to C57BL/6J mice for more than 15 generations. Hemizygous SOD1^{G93A} mice and *Lgals1*$^{+/-}$ mice were crossed to obtain SOD1^{G93A}/*Lgals1*$^{+/-}$ mice, then SOD1^{G93A}/*Lgals1*$^{+/-}$ mice and *Lgals1*$^{+/-}$ mice were crossed to obtain SOD1^{G93A}/*Lgals1*$^{+/+}$ mice and SOD1^{G93A}/*Lgals1*$^{-/-}$ mice. Non-transgenic littermates were used as the wild-type mice. All animals were maintained in an air-conditioned, specific-pathogen-free room with a time-controlled lighting system. The handling and sacrifice of all animals was carried out in accordance with nationally prescribed guidelines, and ethical approval for the study was granted by the Animal Care and Use Committee (Kyushu University, Fukuoka, Japan).

Antibodies

The rabbit polyclonal antibody against recombinant human galectin-1 (anti-rhGAL-1) we used in this study has been described previously [24]. A mouse monoclonal antibody against glial fibrillary acidic protein (anti-GFAP) (G3893, 1:500), a marker for astrocytes,

was obtained from Sigma-Aldrich Japan KK (Tokyo, Japan). A rat monoclonal antibody against CD11b (Ab8878, 1:500), a marker for microglia, was obtained from Abcam KK (Tokyo, Japan). A mouse monoclonal antibody against neurofilament 200 (N5389, 1:500) and a mouse monoclonal antibody against β-actin (A5316, 1:10,000) were obtained from Sigma-Aldrich Japan KK (Tokyo, Japan). Alexa Fluor-labeled secondary antibodies were obtained from Invitrogen Japan (Tokyo, Japan).

Immunohistochemistry

All animals were deeply anesthetized with pentobarbital (50 mg/kg i.p.) and were perfused intracardially with saline followed by cold 4% paraformaldehyde in phosphate-buffered saline (PBS). The lumbar cord was removed, immersed for over 12 h in the same 4% paraformaldehyde fixative at 4 °C, and cryoprotected in 20 and 30% sucrose in PBS for over 12 h at 4 °C. The tissues were embedded in OCT compound (Sakura Finetech, Tokyo, Japan), frozen, and stored at −80 °C until use. Cross sections (20 μm thickness) were cut on a cryostat, and collected as free-floating sections in PBS. Endogenous peroxidase was blocked by 3% H_2O_2 in methanol/PBS (1:1) for 30 min at room temperature (RT). After blocking by Block Ace (Dainippon Pharmaceutical, Osaka, Japan) for 30 min at RT, sections were incubated with appropriately-diluted primary antibody at 4 °C overnight. Then, they were processed using a Vectastain ABC kit (Vector Laboratories, Burlingame, CA, USA) with an appropriate biotinylated secondary antibody. The peroxidase reaction was detected using 3′3′-diaminobenzidine-tetrahydrochloride (Vector Laboratories). Digital images were acquired using an AxioImager A1 microscope equipped with an AxioCam HRc camera and Axiovision 4.8 imaging software (Carl Zeiss Microscopy Co., Ltd., Tokyo, Japan).

Laser scanning confocal immunofluorescence microscopy

Free-floating sections (40 μm) incubated with an appropriate primary antibody were further incubated with an Alexa-Fluor-labeled secondary antibody in a solution containing DAPI (0.05 μg/ml, Sigma-Aldrich). Confocal images were acquired using a laser scanning confocal microscopy system (Axiovert 200M, LSM510 META-V3.2 software, Carl Zeiss Microscopy Co., Ltd.).

Number of motor neurons

We counted the number of motor neurons in the lumbar cord from animals 38 weeks of age. A total of ten sections (20 μm) each spaced at every fifth section of the cord were Nissl stained. Images of these sections were acquired and analyzed using Image J 1.46r (National Institute of Health, Bethesda, MD, USA). Alpha motor neurons were defined by the following criteria: (1) the presence of a large single nucleolus located within the nucleus, surrounded by light blue staining cytoplasm; and (2) a cell soma area in the range 250–1100 μm^2 [25].

Real-time RT-PCR analysis

Total RNA was prepared from whole mouse spinal cord using ISOGEN (Nippongene, Tokyo, Japan). First-strand cDNA, which was synthesized using a High Capacity cDNA Reverse Transcription Kit (Applied Biosystems Japan, Tokyo, Japan) according to the manufacturer's instructions, was subjected to qPCR. All qPCR assays were performed with a Thunderbird™ SYBR® Green qPCR MIX (Toyobo, Osaka, Japan) and a Takara Thermal Cycler Dice® Real Time System (Takara Bio, Shiga, Japan). The primers we

used to quantify the galectin-1 cDNA were 5′-ATCCTCGCTTCAATGCCCATGG-3′ and 5′-GGTGATGCACACCTCTGTGATG-3′. The primers for GAPDH, 5′-AAATGGTGAAGGTCGGTGTG-3′ and 5′-TGAAGGGGTCGTTGATGG-3′ were obtained from Takara Bio. Expression levels were determined by normalization to GAPDH mRNA, and the levels of galectin-1 mRNA relative to the wild-type mice at 20 weeks of age are presented.

Western blotting

Whole spinal cords of mice were homogenized in 400 μl of lysis buffer containing 200 mM Tris-HCl (pH 6.8), 8% sodium dodecyl sulfate (SDS), 40% Glycerol, and 400 mM β-mercaptoethanol using a Potter-type homogenizer. After centrifugation at 10,000 × g for 10 min, the supernatants were collected. The protein concentration in the supernatant was measured using a DC protein assay Kit (Bio-Rad, Tokyo, Japan). Total protein (10 μg each) was separated by SDS polyacrylamide gel electrophoresis (15%). Western blotting analysis was performed using anti-rhGAL-1 (500 ng/ml) according to a previously described method [26]. Recombinant mouse galectin-1 purified from *Escherichia coli* BL21 cells carrying pET8c: rmGal-1 was used as a standard [27]. The density of each band was quantified using Image J 1.46r.

Behavioral study

Body weights and performances in the rotarod test (Model 47600; UGO, Basile, Italy) were assessed once a week. Mice were put on a rotating bar (20 rpm), and the times at which they fell off of the bar were recorded. The trials were performed three times a day, and the longest time was recorded. The time limit of each observation was 300 s. The

time of disease onset was retrospectively determined as the time when the mice reached their peak body weights [28]. The endpoint of the observations was the day when the mouse lost the ability to right itself within 30 s of being placed on its side [29, 30]. The body weight and rotarod test data were collected only from female mice because few male mice having an $SOD1^{G93A}/Lgals1^{-/-}$ genotype were born in our colony. Survival was analyzed in both male and female mice, because it has been reported that there is no gender influence on survival in $SOD1^{G93A}$ mice with a C57BL/6J background [31].

Electron microscopy

The animals were perfused intracardially with saline followed by cold 4% paraformaldehyde and 2.5% glutaraldehyde in PBS. The anterior half of the lumbar cord was prefixed with a fix buffer (2.5% glutaraldehyde, 0.1 M sucrose, 3 mM $CaCl_2$, and 0.1 M sodium cacodylate, pH 7.4) overnight at 4 °C. After being rinsed in PBS, the tissue was postfixed with 1% osmium tetroxide for 2 h, dehydrated in ethanol and propylene oxide, and embedded in DMP30 resin (TAAB Laboratories, Aldermaston, Berkshire, UK). Ultrathin sections (80 nm) were stained with uranyl acetate for 5 min and with lead acetate for 10 min, and then examined with a transmission electron microscope (Tecnai 20; FEI Company Japan Ltd., Tokyo, Japan). Images with axons were taken from four to eight randomly selected sections from each mouse (magnification ×1700) and analyzed using Image J 1.46r. To compare the size of axons, we measured the internal diameters of myelinated axons. These sections contained both cross-sectional and lengthwise axons, and some axons were unclear in their directions. To avoid overestimation caused by confusion regarding its direction, we measured the length of the short side when we put an axon in a box (Figure S1). We counted myelinated axons in the anterior horn and the

anterior root exit zone, which measured more than 1 μm in internal diameter.

Immunoelectron microscopy

The animals were perfused intracardially with saline followed by cold 4% paraformaldehyde and 0.4% glutaraldehyde in PBS. The anterior half of the lumbar cord was prefixed with a fix buffer (4% paraformaldehyde, 0.4% glutaraldehyde, 3.4% sucrose, 3 mM $CaCl_2$, and 0.1 M sodium cacodylate, pH 7.4) for 1 h on ice. After being rinsed in PBS, the spinal cords were incubated in 2.3 M sucrose and then in 20% polyvinylpyrrolidone (Nacalai Tesque, Kyoto, Japan) prepared in 1.8 M sucrose. Ultrathin sections (100 nm) were cut and blocked by Block Ace (Dainippon Pharmaceutical). Sections were incubated with anti-rhGAL-1 overnight at 4°C and then with anti-rabbit IgG-gold (10 nm) (EY Lab, San Mateo, CA, USA). Sections were post-fixed with 2.5% glutaraldehyde in 0.1 M cacodylate buffer, mounted with 0.2 % uranyl acetate in 2% polyvinyl alcohol (Sigma-Aldrich), and examined under the transmission electron microscope (Tecnai 20).

Analysis of axonal transport

We examined axonal transport using Cholera Toxin Subunit B (CTB) conjugated with Alexa Fluor 488 (Invitrogen) as previously described [32, 33] with modifications. Under anesthesia with a mixed anesthetic (medetomidine hydrochloride 0.3 mg/kg, midazolam 4 mg/kg, butorphanol tartrate 5 mg/kg, i.p.), CTB (12.5 μg) was injected into the gastrocnemius muscle using a micro syringe (Hamilton, Reno, NV, USA). The needle was left in place for 1 min to prevent leakage and the injection site was closed surgically. The animals were anesthetized again 48 h later, and the sciatic nerve was

isolated. The isolated nerve was kept in warmed Ringer's solution, and time-lapse imaging was performed using a laser scanning confocal microscopy system (Axiovert 200M, LSM510 META-V3.2 software) with a P-Apochromat 20 × objective (N.A. 0.8). During imaging, nerves were kept in a thermostatic chamber (37 °C). Transport characteristics of individual CTB-labeled vesicles were analyzed using Image J 1.46r. Kymographs were generated using the "Multiple Kymograph" plug-in and the velocity of vesicular movement was measured using "MTrackJ" plug-in. We measured only vesicles that could be tracked over at least three consecutive time points within a single axon. The transport velocity was determined by measuring the distance covered by a vesicle between two consecutive frames.

Statistical analysis

Data are expressed as the mean ± standard error of the mean (SEM). Pairwise comparisons between two groups were performed using the student's *t* test or Wilcoxon test. For multiple comparisons with the three genotypes, we performed one-way ANOVA. Two-way ANOVA was performed for multiple comparisons with genotypes and ages, and the results obtained by standard least squares fits followed by appropriate post-hoc tests are shown. For the analysis of the body weights and rotarod scores that were determined repeatedly in the same subjects, subjects were considered as random effects and two-way ANOVA was performed with the restricted maximal likelihood method. The time of disease onset (peak body weight), time of rotarod failure onset (defined as the week in which a mouse lost the ability to stay on a rotating bar for 300s without recovery during the study period), time at which 10% body weight loss from peak body weight was apparent, and survival time were compared using the Kaplan-

Meier method and log-rank test. The velocity distribution of CTB-labeled vesicles was compared using the Steel-Dwass test. A value of $P < 0.05$ was considered statistically significant. All statistical analyses were carried out using JMP 9.02 software (SAS Institute, Cary, NC, USA).

Results

The expression of galectin-1 changes according to the progression of ALS-like pathologies in SOD1^{G93A} mice

The SOD1^{G93A} mice we used in the present study had a C57BL/6J genetic background and carried low copy numbers of the G93A mutant form of the human *SOD1* gene. These mice exhibited a slow disease progression. At 20 weeks of age, compared with wild-type mice, SOD1^{G93A} mice exhibited no obvious histopathological abnormalities in their spinal cords by hematoxylin and eosin staining (Figure 1**A**, **B**). At 26 weeks of age, extensive vacuoles were observed in their neuropils (Figure 1**C**). At 38 weeks of age, there was marked loss of motor neurons and gliosis in their spinal cords (Figure 1**D**).

To compare the expression patterns of galectin-1 in the spinal cord between wild-type and SOD1^{G93A}/*Lgals1*$^{+/+}$ mice, we performed immunohistochemistry using anti-rhGAL-1. No immunoreactivity (IR) was observed in spinal cords prepared from *Lgals1*$^{-/-}$ and SOD1^{G93A}/*Lgals1*$^{-/-}$ mice, in which a gene encoding galectin-1 was disrupted (Figure 2**A**-**C**), thus confirming the specificity of anti-rhGAL-1. In wild-type mice, galectin-1 IR was detected in cell bodies and dendrites of motor neurons as well as the neuropil in the gray matter of the spinal cord (Figure 2**D**, **E**). In contrast, in the white matter of the spinal cord, galectin-1 IR was selectively detected in axons of motor neurons (Figure 2**D**, **F**). In SOD1^{G93A}/*Lgals1*$^{+/+}$ mice at 20 weeks of age, galectin-1 IR was detected in the gray matter, as in wild-type mice (Figure 2**G**, **H**). However, spheroid-like structures with strong galectin-1 IR were observed only in SOD1^{G93A}/*Lgals1*$^{+/+}$ mice

(Figure 2**G**, **I**), most prominently in their white matter. In SOD1^{G93A}/*Lgals1*$^{+/+}$ mice at 38 weeks of age, galectin-1 IRs were significantly higher in the white matter, especially in the anterior root exit zone, in which glia-like cells exhibited strong gallectin-1 IRs (Figure 2**J**, **L**). In the gray matter, galectin-1 IRs in the neuropil were higher, whereas IRs in the cell bodies of neurons were not evident, probably because of neuronal loss (Figure 2**J**, **K**).

We next examined the localization of galectin-1 in the spinal cord by laser scanning confocal immunofluorescence microscopy. In the anterior root exit zone of wild-type mice, galectin-1 IR was detected in axons of motor neurons (Figure 3**A**). In SOD1^{G93A}/*Lgals1*$^{+/+}$ mice at 20 weeks of age, there was strong galectin-1 IR colocalized with aggregated neurofilaments in swollen axons of motor neurons, namely axonal spheroids, which were often observed in the anterior root exit zone (Figures 3**B** and S2). This indicates that endogenous galectin-1 accumulated in neurofilamentous lesions in SOD1^{G93A}/*Lgals1*$^{+/+}$ mice, as observed in humans with ALS [5]. In SOD1^{G93A}/*Lgals1*$^{-/-}$ mice at 20 weeks of age, large aggregates with neurofilament IR were also found, but the size and intensity of neurofilament IR was apparently decreased compared with those in SOD1^{G93A}/*Lgals1*$^{+/+}$ mice (Figures 3**C** and S2). Again, there was no galectin-1 IR in these aggregates, thus indicating that anti-rhGAL-1 did not bind to non-specific proteins in these aggregates.

In SOD1^{G93A}/*Lgals1*$^{+/+}$ mice at 38 weeks of age, the cells surrounding the axons of motor neurons exhibited galectin-1 IRs, in addition to the motor-neuron axons themselves (Figure 3**D**, **E**). These cells were positive for glial fibrillary acidic protein and were likely activated astrocytes (Figure 3**G**, **H**). Fewer astrocytes were observed in the same region of wild-type mice, and they exhibited weak galectin-1 IR (Figure 3**F**). No galectin-1 IR

was detected in microglia with a weak CD11b IR in wild-type mice (Figure 3**I**). Similarly, no galectin-1 IR was detected in microglia that exhibited strong CD11b IR in SOD1^{G93A}/*Lgals1*$^{+/+}$ mice at 38 weeks of age (Figure 3**J**).

To compare the expression levels of galectin-1 mRNA in the spinal cord between wild-type and SOD1^{G93A}/*Lgals1*$^{+/+}$ mice, we performed quantitative RT-PCR. The relative level of galectin-1 mRNA was significantly higher in SOD1^{G93A}/*Lgals1*$^{+/+}$ mice at 35 weeks of age (Figure 4**A**). Western blotting analysis revealed that the amount of galectin-1 protein was also higher in the spinal cord of SOD1^{G93A}/*Lgals1*$^{+/+}$ mice at 35 weeks of age (Figures 4**B**, **C** and S3), reaching 0.031 ± 0.02% of total protein. It is likely that the elevated levels of galectin-1 mRNA and protein in SOD1^{G93A}/*Lgals1*$^{+/+}$ mice at 35 weeks of age reflect the higher expression of galectin-1 in activated astrocytes as observed in Figure 3 (F-H).

Effects of galectin-1 deficiency in SOD1^{G93A} mice

Next, we examined whether the progression of ALS-like symptoms in SOD1^{G93A} mice was affected by the absence of endogenous galectin-1 protein. The SOD1^{G93A}/*Lgals1*$^{+/+}$ mice we used in the present study started to decrease in body weight around 34 weeks of age and then exhibited rotarod performance declines (Figure 5**A**-**C**). They reached the endpoint of observation around 46 weeks of age (Figure 5**D**). *Lgals1*$^{-/-}$ mice exhibited neither motor dysfunction nor loss of body weight (Figure 5**A**, **B**) and their life spans were not affected over the observation period in this study.

In our comparisons of rotarod scores and body weights between SOD1^{G93A}/*Lgals1*$^{+/+}$ and SOD1^{G93A}/*Lgals1*$^{-/-}$ mice, there was no significant difference

throughout the observation period (Figure 5**A**, **B**). The disease onset (peak body weight) was at 33.9 ± 0.8 weeks in SOD1^{G93A}/*Lgals1*$^{+/+}$ mice and 34.2 ± 0.9 weeks in SOD1^{G93A}/*Lgals1*$^{-/-}$ mice (P = 0.6503) (Figure 5**C**, Table 1). The onset of rotarod failure and 10% body weight loss were similar between the two groups (Figure S4, Table 1). There was also no significant difference in life span, with SOD1^{G93A}/*Lgals1*$^{+/+}$ mice having a life span of 315.6 ± 7.8 days and SOD1^{G93A}/*Lgals1*$^{-/-}$ mice having a life span of 323.6 ± 7.2 days (P = 0.5058) (Figure. 5**D,** Table 1). The number of surviving motor neurons at 38 weeks of age was not different between the two groups (Figure. 5**E**).

Galectin-1 deficiency improves axonal swelling of motor neurons in presymptomatic SOD1^{G93A} mice

As shown in Figures 2–4, the expression of galectin-1 was altered during the progression of ALS-like symptoms in SOD1^{G93A} mice. The predominant expression of galectin-1 was in motor neurons before the development of ALS-like symptoms, whereas its expression in astrocytes was markedly higher after the development of ALS-like symptoms.

To examine how galectin-1 deficiency in motor neurons affects axonal pathophysiology in presymptomatic SOD1^{G93A} mice, we performed electron microscopic observations of the spinal cord. Myelinated axons in *Lgals1*$^{-/-}$ mice had essentially the same shape and size as those in wild-type mice (Figure 6**A**, **B**). In SOD1^{G93A}/*Lgals1*$^{+/+}$ mice at 20 weeks of age, large swollen axons were observed and they were filled with tangled neurofilaments and large vacuoles together with a few normal-shaped mitochondria (Figures 6**A**, **B,** and S5). Immunoelectron microscopy using anti-rhGAL-1

revealed that galectin-1 IRs were mostly detected alongside tangled neurofilaments, with few in vacuoles (Figure 6**C**). In SOD1^{G93A}/*Lgals1*$^{-/-}$ mice at 20 weeks of age, swollen axons were still present but their size and the number of vacuoles was apparently reduced (Figures 6**A**, **B** and S5). To compare the size of axons, we measured the internal diameters of myelinated axons. In both SOD1^{G93A}/*Lgals1*$^{+/+}$ and SOD1^{G93A}/*Lgals1*$^{-/-}$ mice at 20 weeks of age, the numbers of myelinated axons were the same as in wild-type mice (Figure 6**D**). Most of the myelinated axons in wild-type mice had internal diameters less than 4 μm (Figures 6**E** and S6). In SOD1^{G93A}/*Lgals1*$^{+/+}$ mice, axons having large diameters, especially over 6 μm, were notably more prevalent, and such large axons were less frequently observed in SOD1^{G93A}/*Lgals1*$^{-/-}$ mice (Figures 6**E** and S6). When we compared the diameters of axons with internal diameters larger than 4 μm, the diameters of these axons in SOD1^{G93A}/*Lgals1*$^{-/-}$ were significantly smaller compared with those in SOD1^{G93A}/*Lgals1*$^{+/+}$ mice (Figure 6**F**). Furthermore, accumulation of vacuoles in swollen axons was significantly less frequently observed in SOD1^{G93A}/*Lgals1*$^{-/-}$ mice (Figures 6**B**, **G**, S5 and S6).

Pathological study suggested that galectin-1 deficiency improved early axonal changes in SOD1^{G93A} mice. We next examined whether axonal functions can be affected by galectin-1 deficiency. We examined axonal transport using Cholera Toxin Subunit B (CTB) conjugated to Alexa Fluor 488. CTB is a widely used retrograde neuronal tracer, and we could detect fluorescently labeled motor neurons in the lumbar cord after injection of CTB-dye into the gastrocnemius muscle (Figure 7**A**, **B**). Using time-lapse imaging of the isolated sciatic nerve, we measured the mobility of retrogradely transported, CTB-labeled vesicles (Videos S1-3). Axonal transport was significantly impaired in presymptomatic SOD1^{G93A}/*Lgals1*$^{+/+}$ mice compared with wild-type mice. The velocity

distribution of CTB-labeled vesicles was significantly different between SOD1^{G93A}/*Lgals1*$^{-/-}$ and SOD1^{G93A}/*Lgals1*$^{+/+}$ mice (Figure 7**D**, **E**), although the average velocity of vesicles in each mouse was not significantly different between SOD1^{G93A}/*Lgals1*$^{+/+}$ and SOD1^{G93A} /*Lgals1*$^{-/-}$ mice (Figure 7**F**). We suggest that, at least, retrograde axonal transport was partially improved in SOD1^{G93A}/*Lgals1*$^{-/-}$ mice compared with SOD1^{G93A}/*Lgals1*$^{+/+}$ mice.

Discussion

In the present study, we demonstrated that galectin-1 accumulates in neurofilamentous lesions in SOD1^{G93A} mice as previously reported in humans with ALS. Galectin-1 accumulation occurred before the development of ALS-like symptoms and improvements in axonal swelling were associated with galectin-1 deficiency. Furthermore, we found that astrocytes surrounding the degenerating axons of motor neurons express high levels of galectin-1 in symptomatic SOD1^{G93A} mice.

In the spinal cords of wild-type animals, galectin-1 was abundantly expressed in motor neurons, and its relative expression level was higher than 0.02% of total protein (Figure 4**C**). However, its functions in the motor-neuron system are largely unknown. In the adult rat nervous system, galectin-1 mRNA has been predominantly observed in neuronal cell bodies of cranial nerve motor nuclei and spinal motor neurons [34]. Because expression of galectin-1 mRNA is transiently increased after axotomy of facial nerve and spinal motor neurons, galectin-1 may have roles in motor nerve regeneration after injury [34, 35]. Although *Lgals1*$^{-/-}$ mice do not exhibit motor dysfunction, at least under normal conditions, it has been reported that they show deficient olfactory networks [12], reduced thermal sensitivity [36], and impaired spatial and contextual memory formation [37]. In the present study, we showed that the expression and distribution of galectin-1 in the spinal cord are greatly altered during the progression of ALS-like symptoms. It is likely that galectin-1 expressed in motor neurons and astrocytes has different functions and both are associated with axonal degeneration in SOD1^{G93A} mice.

There is accumulating evidence from ALS patients and animal models that axonal degeneration begins at very early stages and proceeds independently from the

degeneration of cell bodies [38, 39]. Sasaki et al. [40] reported that the earliest morphological changes in SOD1^{G93A} mice with a low copy number of transgenes are mild swelling and vacuolation of mitochondria in proximal axons of motor neurons. Vacuolar changes then become increasingly prominent and accumulated neurofilaments are seen in close proximity to vacuoles and in swollen axons. We found the diameters of swollen motor axons in the spinal cord were significantly smaller in SOD1^{G93A}/*Lgals1*$^{-/-}$ mice compared with SOD1^{G93A}/*Lgals*$^{+/+}$ mice, thus demonstrating that galectin-1 is a major accumulating component in swollen motor axons in presymptomatic SOD1^{G93A} mice. Additionally, there was less accumulation of vacuoles in SOD1^{G93A}/*Lgals1*$^{-/-}$ mice. Vacuoles observed in presymptomatic mutant SOD1 transgenic mice are generally recognized to be derived from degenerating mitochondria [40-43], even though some reports propose that vacuoles are derived from the endoplasmic reticulum [44]. It has been reported that autophagic vacuoles also accumulate in myelinated axons of motor neurons in SOD1^{G93A} mice, especially in late stages of the disease [45]. We observed accumulating vacuoles in axons before the development of ALS-like symptoms, thus suggesting that these vacuoles are mostly derived from degenerating mitochondria.

Using immunoelectron microscopy, galectin-1 was detected alongside tangled neurofilaments in axonal spheroids. It has also been reported that galectin-1 is bound to neurofilaments that have accumulated in axonal spheroids in humans with ALS [5]. It is possible that galectin-1 promotes aggregation of neurofilaments via its ability to bind various molecules and form cross-linkages. Another possibility is that galectin-1 itself aggregates following ROS production from damaged mitochondria [46], because galectin-1 has six cysteine residues in the molecule and abnormal oxidation can occur. If these aggregates trap mitochondria, it leads to mitochondrial accumulation and

vacuolation in motor axons because damaged mitochondria are transported to cell bodies for repair or autophagy [47] and entrapment of mitochondria in axons possibly exacerbates their degeneration.

In human ALS patients, large vacuolated mitochondria in motor axons, like those observed in SOD1^{G93A} mice, have not been detected. However, morphological and functional abnormalities have been reported [48, 49]. In SOD1^{G93A} mice, vacuolation is a transient process that is most prominent during the onset of muscle weakness and disappears at the end stages of ALS-like symptom progression (Figure 1**C**, **D**), probably as the result of severe axonal degeneration [42]. Because pathological examination of humans with ALS is generally performed at the terminal stage of the disease, it is possible that vacuolation is also an essential process in the early stages of ALS in humans [42]. Accumulation of galectin-1 in neurofilamentous lesions has been observed in both sporadic and familial ALS patients with the *SOD1* mutation (A4V) [5], suggesting that galectin-1 is involved in the early pathogenesis of both sporadic and familial ALS cases, just as we observed in SOD1^{G93A} mice.

Although galectin-1 deficiency was associated with fewer pathological changes of axons of motor neurons in presymptomatic SOD1^{G93A} mice, there were no significant differences in the disease progression between SOD1^{G93A}/*Lgals1*$^{+/+}$ and SOD1^{G93A}/*Lgals1*$^{-/-}$ mice at any time point. One possibility is that the contribution of galectin-1 accumulation to the phenotype of SOD1^{G93A} is not extensive and the toxicity of mutant SOD1 exceeds the effects of galectin-1 deficiency in motor neurons. Another possibility is loss of the protective role of galectin-1 expressed in astrocytes. Administration of oxidized galectin-1 monomers has been shown to be neuroprotective in mutant SOD1 transgenic mice [21]. Additionally, it has been reported that reduced

galectin-1 induces differentiation of cultured astrocytes, which leads to production of brain-derived neurotrophic factor [50]. Recently, it was reported that galectin-1 secreted from astrocytes deactivates classically activated microglia (M1) and protects against inflammation-induced neurodegeneration in murine experimental autoimmune encephalitis, which is a model of multiple sclerosis [51]. In symptomatic $SOD1^{G93A}$ mice, galectin-1 expressed in astrocytes may also have neuroprotective effects. Conditional inactivation of galectin-1 either in motor neurons or astrocytes in future studies would provide important insights into the possible role of galectin-1 in these cell types.

We showed that galectin-1 is involved in the pathogenesis of ALS throughout the disease course. Galectin-1 accumulation in motor axons was associated with early processes of axonal degeneration. Further functional investigation of galectin-1 expressed in astrocytes may provide a potential novel therapy for ALS.

Acknowledgments

This work was supported by the Japan Society for the Promotion of Science KAKENHI (Grant Numbers 22221004 & 25110724) and the Kyushu University Global COE Program (Cell-fate Decision: Function and Dysfunction in Homeostasis). We thank Dr. Françoise Poirier (Department of Developmental Biology, Institute Jacques Monod, Universities Paris 6 and Paris 7, France) for kindly providing *Lgals1*-knockout mice, Mr Ryo Ugawa (Laboratory for Technical Support, Medical Institute of Bioregulation, Kyushu University, Kyushu, Japan) for electron microscopy, and Ms S. Kitamura and Ms K. Asakawa and Ms T. Kuwano for their technical assistance.

Conflicts of interest

The authors declare no competing financial interests.

Author contributions

Y.K., K.S., J. K., and Y.N. designed research; Y.K., K.S., and K.K. performed the research; T.K. and H.H. provided new reagents; Y.K., K.S., and Y.N. analyzed the data; Y.K., K.S., J. K., and Y.N. wrote the paper.

References

1 Pratt AJ, Getzoff ED, Perry JJ. Amyotrophic lateral sclerosis: update and new developments. Degener Neurol Neuromuscul Dis 2012; 2012: 1-14

2 Hirano A, Nakano I, Kurland LT, Mulder DW, Holley PW, Saccomanno G. Fine structural study of neurofibrillary changes in a family with amyotrophic lateral sclerosis. J Neuropathol Exp Neurol 1984; 43: 471-80

3 Tu PH, Raju P, Robinson KA, Gurney ME, Trojanowski JQ, Lee VM. Transgenic mice carrying a human mutant superoxide dismutase transgene develop neuronal cytoskeletal pathology resembling human amyotrophic lateral sclerosis lesions. Proc Natl Acad Sci U S A 1996; 93: 3155-60

4 Xiao S, McLean J, Robertson J. Neuronal intermediate filaments and ALS: a new look at an old question. Biochim Biophys Acta 2006; 1762: 1001-12

5 Kato T, Kurita K, Seino T, Kadoya T, Horie H, Wada M, Kawanami T, Daimon M, Hirano A. Galectin-1 is a component of neurofilamentous lesions in sporadic and familial amyotrophic lateral sclerosis. Biochem Biophys Res Commun 2001; 282: 166-72

6 Barondes SH, Castronovo V, Cooper DN, Cummings RD, Drickamer K, Feizi T, Gitt MA, Hirabayashi J, Hughes C, Kasai K, et al. Galectins: a family of animal β-galactoside-binding lectins. Cell 1994; 76: 597-8

7 Elola MT, Wolfenstein-Todel C, Troncoso MF, Vasta GR, Rabinovich GA. Galectins: matricellular glycan-binding proteins linking cell adhesion, migration, and survival. Cell Mol Life Sci 2007; 64: 1679-700

8 Boscher C, Dennis JW, Nabi IR. Glycosylation, galectins and cellular signaling. Curr

Opin Cell Biol 2011; 23: 383-92

9 Ito K, Stannard K, Gabutero E, Clark AM, Neo SY, Onturk S, Blanchard H, Ralph SJ. Galectin-1 as a potent target for cancer therapy: role in the tumor microenvironment. Cancer Metastasis Rev 2012; 31: 763-78

10 Cedeno-Laurent F, Dimitroff CJ. Galectin-1 research in T cell immunity: past, present and future. Clin Immunol 2012; 142: 107-16

11 Park JW, Voss PG, Grabski S, Wang JL, Patterson RJ. Association of galectin-1 and galectin-3 with Gemin4 in complexes containing the SMN protein. Nucleic Acids Res 2001; 29: 3595-602

12 Puche AC, Poirier F, Hair M, Bartlett PF, Key B. Role of galectin-1 in the developing mouse olfactory system. Dev Biol 1996; 179: 274-87

13 Sakaguchi M, Shingo T, Shimazaki T, Okano HJ, Shiwa M, Ishibashi S, Oguro H, Ninomiya M, Kadoya T, Horie H, Shibuya A, Mizusawa H, Poirier F, Nakauchi H, Sawamoto K, Okano H. A carbohydrate-binding protein, Galectin-1, promotes proliferation of adult neural stem cells. Proc Natl Acad Sci U S A 2006; 103: 7112-7

14 Sakaguchi M, Okano H. Neural stem cells, adult neurogenesis, and galectin-1: from bench to bedside. Dev Neurobiol 2012; 72: 1059-67

15 Kajitani K, Nomaru H, Ifuku M, Yutsudo N, Dan Y, Miura T, Tsuchimoto D, Sakumi K, Kadoya T, Horie H, Poirier F, Noda M, Nakabeppu Y. Galectin-1 promotes basal and kainate-induced proliferation of neural progenitors in the dentate gyrus of adult mouse hippocampus. Cell Death Differ 2009; 16: 417-27

16 Imaizumi Y, Sakaguchi M, Morishita T, Ito M, Poirier F, Sawamoto K, Okano H. Galectin-1 is expressed in early-type neural progenitor cells and down-regulates

neurogenesis in the adult hippocampus. Mol Brain 2011; 4: 7

17 Inagaki Y, Sohma Y, Horie H, Nozawa R, Kadoya T. Oxidized galectin-1 promotes axonal regeneration in peripheral nerves but does not possess lectin properties. Eur J Biochem 2000; 267: 2955-64

18 Kadoya T, Horie H. Structural and functional studies of galectin-1: a novel axonal regeneration-promoting activity for oxidized galectin-1. Curr Drug Targets 2005; 6: 375-83

19 Horie H, Kadoya T, Hikawa N, Sango K, Inoue H, Takeshita K, Asawa R, Hiroi T, Sato M, Yoshioka T, Ishikawa Y. Oxidized galectin-1 stimulates macrophages to promote axonal regeneration in peripheral nerves after axotomy. J Neurosci 2004; 24: 1873-80

20 Lerman BJ, Hoffman EP, Sutherland ML, Bouri K, Hsu DK, Liu FT, Rothstein JD, Knoblach SM. Deletion of galectin-3 exacerbates microglial activation and accelerates disease progression and demise in a $SOD1^{G93A}$ mouse model of amyotrophic lateral sclerosis. Brain Behav 2012; 2: 563-75

21 Chang-Hong R, Wada M, Koyama S, Kimura H, Arawaka S, Kawanami T, Kurita K, Kadoya T, Aoki M, Itoyama Y, Kato T. Neuroprotective effect of oxidized galectin-1 in a transgenic mouse model of amyotrophic lateral sclerosis. Exp Neurol 2005; 194: 203-11

22 Alexander GM, Erwin KL, Byers N, Deitch JS, Augelli BJ, Blankenhorn EP, Heiman-Patterson TD. Effect of transgene copy number on survival in the G93A SOD1 transgenic mouse model of ALS. Brain Res Mol Brain Res 2004; 130: 7-15

23 Poirier F, Robertson EJ. Normal development of mice carrying a null mutation in the gene encoding the L14 S-type lectin. Development 1993; 119: 1229-36

24 Horie H, Inagaki Y, Sohma Y, Nozawa R, Okawa K, Hasegawa M, Muramatsu N, Kawano H, Horie M, Koyama H, Sakai I, Takeshita K, Kowada Y, Takano M, Kadoya T. Galectin-1 regulates initial axonal growth in peripheral nerves after axotomy. J Neurosci 1999; 19: 9964-74

25 Drachman DB, Frank K, Dykes-Hoberg M, Teismann P, Almer G, Przedborski S, Rothstein JD. Cyclooxygenase 2 inhibition protects motor neurons and prolongs survival in a transgenic mouse model of ALS. Ann Neurol 2002; 52: 771-8

26 Tsuchimoto D, Sakai Y, Sakumi K, Nishioka K, Sasaki M, Fujiwara T, Nakabeppu Y. Human APE2 protein is mostly localized in the nuclei and to some extent in the mitochondria, while nuclear APE2 is partly associated with proliferating cell nuclear antigen. Nucleic Acids Res 2001; 29: 2349-60

27 Miura T, Takahashi M, Horie H, Kurushima H, Tsuchimoto D, Sakumi K, Nakabeppu Y. Galectin-1β, a natural monomeric form of galectin-1 lacking its six amino-terminal residues promotes axonal regeneration but not cell death. Cell Death Differ 2004; 11: 1076-83

28 Boillee S, Yamanaka K, Lobsiger CS, Copeland NG, Jenkins NA, Kassiotis G, Kollias G, Cleveland DW. Onset and progression in inherited ALS determined by motor neurons and microglia. SCIENCE 2006; 312: 1389-92

29 Ludolph AC, Bendotti C, Blaugrund E, Chio A, Greensmith L, Loeffler JP, Mead R, Niessen HG, Petri S, Pradat PF, Robberecht W, Ruegg M, Schwalenstocker B, Stiller D, van den Berg L, Vieira F, von Horsten S. Guidelines for preclinical animal research in ALS/MND: A consensus meeting. Amyotroph Lateral Scler 2010; 11: 38-45

30 Scott S, Kranz JE, Cole J, Lincecum JM, Thompson K, Kelly N, Bostrom A,

Theodoss J, Al-Nakhala BM, Vieira FG, Ramasubbu J, Heywood JA. Design, power, and interpretation of studies in the standard murine model of ALS. Amyotroph Lateral Scler 2008; 9: 4-15

31 Heiman-Patterson TD, Deitch JS, Blankenhorn EP, Erwin KL, Perreault MJ, Alexander BK, Byers N, Toman I, Alexander GM. Background and gender effects on survival in the TgN(SOD1-G93A)1Gur mouse model of ALS. J Neurol Sci 2005; 236: 1-7

32 Marinkovic P, Reuter MS, Brill MS, Godinho L, Kerschensteiner M, Misgeld T. Axonal transport deficits and degeneration can evolve independently in mouse models of amyotrophic lateral sclerosis. Proc Natl Acad Sci U S A 2012; 109: 4296-301

33 Bilsland LG, Sahai E, Kelly G, Golding M, Greensmith L, Schiavo G. Deficits in axonal transport precede ALS symptoms in vivo. Proc Natl Acad Sci U S A 2010; 107: 20523-8

34 Akazawa C, Nakamura Y, Sango K, Horie H, Kohsaka S. Distribution of the galectin-1 mRNA in the rat nervous system: its transient upregulation in rat facial motor neurons after facial nerve axotomy. Neuroscience 2004; 125: 171-8

35 McGraw J, McPhail LT, Oschipok LW, Horie H, Poirier F, Steeves JD, Ramer MS, Tetzlaff W. Galectin-1 in regenerating motoneurons. Eur J Neurosci 2004; 20: 2872-80

36 McGraw J, Gaudet AD, Oschipok LW, Steeves JD, Poirier F, Tetzlaff W, Ramer MS. Altered primary afferent anatomy and reduced thermal sensitivity in mice lacking galectin-1. Pain 2005; 114: 7-18

37 Sakaguchi M, Arruda-Carvalho M, Kang NH, Imaizumi Y, Poirier F, Okano H,

Frankland PW. Impaired spatial and contextual memory formation in galectin-1 deficient mice. Mol Brain 2011; 4: 33

38 Fischer LR, Culver DG, Tennant P, Davis AA, Wang M, Castellano-Sanchez A, Khan J, Polak MA, Glass JD. Amyotrophic lateral sclerosis is a distal axonopathy: evidence in mice and man. Exp Neurol 2004; 185: 232-40

39 Fischer LR, Glass JD. Axonal degeneration in motor neuron disease. Neurodegener Dis 2007; 4: 431-42

40 Sasaki S, Warita H, Abe K, Iwata M. Slow component of axonal transport is impaired in the proximal axon of transgenic mice with a G93A mutant SOD1 gene. Acta Neuropathol 2004; 107: 452-60

41 Wong PC, Pardo CA, Borchelt DR, Lee MK, Copeland NG, Jenkins NA, Sisodia SS, Cleveland DW, Price DL. An adverse property of a familial ALS-linked SOD1 mutation causes motor neuron disease characterized by vacuolar degeneration of mitochondria. Neuron 1995; 14: 1105-16

42 Kong J, Xu Z. Massive mitochondrial degeneration in motor neurons triggers the onset of amyotrophic lateral sclerosis in mice expressing a mutant SOD1. J Neurosci 1998; 18: 3241-50

43 Parone PA, Da Cruz S, Han JS, McAlonis-Downes M, Vetto AP, Lee SK, Tseng E, Cleveland DW. Enhancing mitochondrial calcium buffering capacity reduces aggregation of misfolded SOD1 and motor neuron cell death without extending survival in mouse models of inherited amyotrophic lateral sclerosis. J Neurosci 2013; 33: 4657-71

44 Dal Canto MC, Gurney ME. Neuropathological changes in two lines of mice carrying a transgene for mutant human Cu,Zn SOD, and in mice overexpressing wild type

human SOD: a model of familial amyotrophic lateral sclerosis (FALS). Brain Res 1995; 676: 25-40

45 Zhang X, Li L, Chen S, Yang D, Wang Y, Zhang X, Wang Z, Le W. Rapamycin treatment augments motor neuron degeneration in $SOD1^{G93A}$ mouse model of amyotrophic lateral sclerosis. Autophagy 2011; 7: 412-25

46 Panov A, Kubalik N, Zinchenko N, Hemendinger R, Dikalov S, Bonkovsky HL. Respiration and ROS production in brain and spinal cord mitochondria of transgenic rats with mutant G93a Cu/Zn-superoxide dismutase gene. Neurobiol Dis 2011; 44: 53-62

47 Miller KE, Sheetz MP. Axonal mitochondrial transport and potential are correlated. J Cell Sci 2004; 117: 2791-804

48 Wiedemann FR, Manfredi G, Mawrin C, Beal MF, Schon EA. Mitochondrial DNA and respiratory chain function in spinal cords of ALS patients. J Neurochem 2002; 80: 616-25

49 Sasaki S, Iwata M. Mitochondrial alterations in the spinal cord of patients with sporadic amyotrophic lateral sclerosis. J Neuropathol Exp Neurol 2007; 66: 10-6

50 Sasaki T, Hirabayashi J, Manya H, Kasai K, Endo T. Galectin-1 induces astrocyte differentiation, which leads to production of brain-derived neurotrophic factor. Glycobiology 2004; 14: 357-63

51 Starossom SC, Mascanfroni ID, Imitola J, Cao L, Raddassi K, Hernandez SF, Bassil R, Croci DO, Cerliani JP, Delacour D, Wang Y, Elyaman W, Khoury SJ, Rabinovich GA. Galectin-1 deactivates classically activated microglia and protects from inflammation-induced neurodegeneration. Immunity 2012; 37: 249-63

Figure Legends

Figure 1. H&E staining of the motor-neuron area in the lumbar cord. (**A**) Staining in wild-type mice at 40 weeks of age. (**B**)-(**D**) Staining in SOD1^{G93A} mice. (**B**) At 20 weeks of age, there were no obvious histopathological abnormalities. (**C**) At 26 weeks of age, viable large motor neurons remained (arrows), but there were many vacuoles (arrowheads) in the neuropil. (**D**) At 38 weeks of age, there was both marked loss of motor neurons and gliosis (dashed arrows). Scale bars, 50 μm.

Figure 2. Immunohistochemical detection of galectin-1 in the mouse lumbar cord. (**A**) – (**C**) Images acquired by differential interference contrast microscopy. Wild-type mice (**A**) exhibited strong galectin-1 IRs in the spinal cord. No immunoreactivity was detected in *Lgals1*$^{-/-}$ mice (**B**) and SOD1^{G93A}/*Lgals1*$^{-/-}$ mice (**C**). (**D**)–(**F**) In wild-type mice at 40 weeks of age, galectin-1 IR was detected in cell bodies, dendrites of motor neurons, gray-matter neuropil (**E**), and axons in the white matter (**F**). (**G**)–(**I**) In SOD1^{G93A}/*Lgals1*$^{+/+}$ mice at 20 weeks of age, spheroid-like structures with strong galectin-1 IR were found especially in the anterior root exit zone (**I**, arrow), whereas essentially the same galectin-1 IR was found in the cell bodies of motor neurons of both SOD1^{G93A}/*Lgals1*$^{+/+}$ and wild-type mice (**H**). (**J**)–(**L**) In SOD1^{G93A}/*Lgals1*$^{+/+}$ mice at 38 weeks of age, the distribution of the galectin-1 IR in the anterior root exit zone was significantly altered (**L**) and galectin-1 IR in the cell bodies of motor neurons was not evident (**K**), probably because of neuronal loss. Scale bars, 100 μm (**A**-**C**, **D**, **G**, **J**), 50 μm (**E**, **F**, **H**, **I**, **K**, **L**).

Figure 3. Localization of galectin-1 in the spinal cord observed by laser scanning

confocal immunofluorescence microscopy. (**A)**–(**E**) Double immunofluorescence staining of lumbar cord with anti-neurofilament (green) and anti-rhGAL-1 (red) antibodies. (**A**) Galectin-1 IR was detected in the axons of motor neurons in the anterior root exit zone of wild-type mice at 40 weeks of age. (**B**) In SOD1^{G93A}/*Lgals1*$^{+/+}$ mice at 20 weeks of age, strong galectin-1 IR was colocalized with aggregated neurofilaments. (**C**) In SOD1^{G93A}/*Lgals1*$^{-/-}$ mice at 20 weeks of age, aggregated neurofilaments were still present but clearly reduced in size. No galectin-1 IR was detected. (**D)**–(**E**) In SOD1^{G93A}/*Lgals1*$^{+/+}$ mice at 38 weeks of age, galectin-1 IRs were detected in cells surrounding the axons of motor neurons in addition to in their axons. (**F)**–(**H**) Double immunofluorescence staining of lumbar cord with anti-GFAP (green) and anti-rhGAL-1 (red) antibodies. (**F**) There were a few astrocytes with weak galectin-1 IR in the anterior root exit zone of wild-type mice at 40 weeks of age. (**G)**–(**H**) In SOD1^{G93A}/*Lgals1*$^{+/+}$ mice at 38 weeks of age, astrocytes surrounding the axons of motor neurons exhibited strong galectin-1 IR. (**I)**–(**J**) Double immunofluorescent staining with anti-CD11b (green) and anti-rhGAL-1 (red) antibodies. (**I**) Microglia exhibited weak CD11b IR and no galectin-1 IR in wild-type mice at 40 weeks of age. **(J)** Microglia exhibited strong CD11b IR and no galectin-1 IR in SOD1^{G93A}/*Lgals1*$^{+/+}$ mice at 38 weeks of age. Cell nuclei were counter-stained with DAPI (blue). Scale bars, 50 μm (**A**–**D**, **F**, **G**), 20 μm (**E**, **H**, **I**, **J**).

Figure 4. Levels of galectin-1 mRNA and protein in the spinal cord increased during the progression of ALS-like pathologies. (**A**) Quantitative RT-PCR using total RNA prepared from the whole spinal cord. The level of galectin-1 mRNA relative to wild-type mice at 20 weeks of age was significantly higher in SOD1^{G93A}/*Lgals1*$^{+/+}$ mice at 35 weeks of age in comparison to the others (n = 3 at 20 and 26 weeks of age, n = 5 at 35 weeks of age).

The relative ratio of galectin-1 mRNA in SOD1^{G93A}/*Lgals1*$^{+/+}$ mice to that in wild-type mice at the same age is shown in parentheses. **P* = 0.0042 (vs 20 weeks SOD1^{G93A}/*Lgals1*$^{+/+}$), 0.0276 (vs 26 weeks SOD1^{G93A}/*Lgals1*$^{+/+}$), 0.0135 (vs 35 weeks wild-type), two-way ANOVA (*P* = 0.0155) followed by individual post hoc student's *t* test. (**B**) Quantitative western blotting of galectin-1 in extracts prepared from whole spinal cord. The amount of galectin-1 protein (ng per total 10 μg protein) was determined using recombinant mouse galectin-1 as a standard. (**C**) At 35 weeks of age, the amount of galectin-1 protein in SOD1^{G93A}/*Lgals1*$^{+/+}$ mice was significantly higher than that in wild-type mice (*n* = 3 in each group, see Figure S3). **P* = 0.0433, student's *t* test. Error bars show the mean ± SEM.

Figure 5. Progression of ALS-like symptoms in SOD1^{G93A}/*Lgals1*$^{+/+}$ and SOD1^{G93A}/*Lgals1*$^{-/-}$ mice. (**A**) Changes in body weight. Wild-type (*n* =5) and *Lgals1*$^{-/-}$ mice (*n* = 3) did not exhibit loss of body weight throughout the observation period. There was no statistical difference in body weight between SOD1^{G93A}/*Lgals1*$^{+/+}$ mice (*n* = 11) and SOD1^{G93A}/*Lgals1*$^{-/-}$ mice (*n* = 11) throughout the observation period (two-way ANOVA: genotype, *P* = 0.8467; week *P* < 0.0001; interaction, *P* = 0.5395). (**B**) Changes in motor function as evaluated by the rotarod test. Wild-type (*n* =5) and *Lgals1*$^{-/-}$ mice (*n* = 3) exhibited no motor dysfunction throughout the observation period. There was no statistical difference in rotarod performance between SOD1^{G93A}/*Lgals1*$^{+/+}$ mice (*n* = 11) and SOD1^{G93A}/*Lgals1*$^{-/-}$ mice (*n* = 11) throughout the observation period (two-way ANOVA: genotype, *P* = 0.9442; week *P* < 0.0001; interaction, *P* = 0.9442). (**C**) Kaplan-Meier graph showing the disease onset (peak body weight). There was no statistical difference between SOD1^{G93A}/*Lgals1*$^{+/+}$ mice (*n* = 11) and SOD1^{G93A}/*Lgals1*$^{-/-}$ mice (*n* =

11) (P = 0.6503, log-rank test). (**D**) Kaplan-Meier survival plots. There was no statistical difference in survival time between SOD1^{G93A}/*Lgals1*$^{+/+}$ mice (n = 16) and SOD1^{G93A}/*Lgals1*$^{-/-}$ mice (n = 16) (P = 0.5058, log-rank test). (**E**) Number of motor neurons in the lumbar cord at 38 weeks of age. The number of surviving motor neurons was significantly lower in both SOD1^{G93A}/*Lgals1*$^{+/+}$ mice (n = 5) and SOD1^{G93A}/*Lgals1*$^{-/-}$ mice (n = 5) compared with wild-type mice (n = 4). *P < 0.05, one-way ANOVA (P = 0.0109) followed by individual post hoc Tukey's HSD test. Error bars show the mean ± SEM.

Figure 6. Electron microscopy of myelinated axons in the lumbar cord. (**A**) Toluidine blue staining of sections for electron microscopy. Scale bars, 50 μm. (**B**) Electron micrograph of myelinated axons in the anterior horn. The shape and size of myelinated axons in *Lgals1*$^{-/-}$ mice were the same as those in wild-type mice. In SOD1^{G93A}/*Lgals1*$^{+/+}$ mice at 20 weeks of age, there were many large swollen axons and they were filled with tangled neurofilaments (arrows) and large vacuoles (arrowheads), together with a few normal-shaped mitochondria (dashed arrows). In SOD1^{G93A}/*Lgals1*$^{-/-}$ mice at 20 weeks of age, diameters of swollen axons were smaller and accumulations of vacuoles were less frequently observed compared with SOD1^{G93A}/*Lgals1*$^{+/+}$ mice. Higher magnification images for SOD1^{G93A}/*Lgals1*$^{+/+}$ and SOD1^{G93A}/*Lgals1*$^{-/-}$ mice are shown in the bottom. Scale bars, 5 μm (top), 1 μm (bottom). (**C**) Immunoelectron microscopy of swollen axon in SOD1^{G93A}/*Lgals1*$^{+/+}$ mice using anti-rhGAL-1. Gold particles (white arrow heads) were detected alongside tangled neurofilaments. Asterisks indicate vacuoles and the white dashed arrow shows a normal-shaped example mitochondrion. Scale bar, 100 nm. (**D**) Number of axons in the lumbar cord. There was no significant difference in the

number of myelinated axons among wild-type, SOD1^{G93A}/*Lgals1*$^{+/+}$ and SOD1^{G93A}/*Lgals1*$^{-/-}$ mice at 20 weeks of age (n = 3 mice in each group). Error bars show the mean ± SEM. n.s., not significant, one-way ANOVA (P = 0.4234). (**E**) Frequency distribution of the diameters of the axons. Internal diameters of myelinated axons in wild-type mice were mostly smaller than 4 μm. In SOD1^{G93A}/*Lgals1*$^{+/+}$ mice, swollen axons having larger diameters, especially over 6 μm, were notably more prevalent. In SOD1^{G93A}/*Lgals1*$^{-/-}$ mice, such swollen axons were less frequently observed. Three mice were examined in each group, and the total numbers of axons examined were 318 axons in wild-type, 911 axons in SOD1^{G93A}/*Lgals1*$^{+/+}$, and 1071 axons in SOD1^{G93A}/*Lgals1*$^{-/-}$. Error bars show the mean ± SEM. (F) Box plots showing the distribution of the internal diameters of swollen axons (dot) larger than 4 μm. The sizes of swollen axons with a diameter ≧4 μm were significantly smaller in SOD1^{G93A}/*Lgals1*$^{-/-}$ mice (n = 134 axons from 3 mice) compared with SOD1^{G93A}/*Lgals1*$^{+/+}$ mice (n = 125 axons from 3 mice). The box indicates 25 to 75% quartiles of the samples with a median line, and the vertical lines show the smallest diameter, 10% quartile, 90% quartile, 97.5% quartile and the largest diameter of any axon in each group, starting at the left. **P < 0.0001, Wilcoxon test. (**G**) The ratio of axons that contain vacuoles in the swollen axons. Most of the swollen axons in SOD1^{G93A}/*Lgals1*$^{+/+}$ mice contained vacuoles, but these vacuoles were less frequently observed in SOD1^{G93A}/*Lgals1*$^{-/-}$ mice (n = 3 mice in each group). Error bars show the mean ± SEM. *P < 0.05, student's t test.

Figure 7. Analysis of axonal transport using Cholera Toxin Subunit B (CTB). (**A**)–(**B**) Detection of CTB-dye in the lumbar cord 5 days after injection into the gastrocnemius muscle in wild-type mice. Fluorescent signals were detected in motor neurons only on

the injected side. (**C**) Representative kymographs showing the mobility of CTB-labeled vesicles in the sciatic nerve. (**D**)–(**F**) Analysis of the mobility of vesicles that were retrogradely transported in the isolated sciatic nerve (28 weeks of age). (**D**) Histograms of the velocity of each CTB-labeled vesicle, showing a faster peak velocity and median velocity (arrows) in SOD1^{G93A} /*Lgals1*$^{-/-}$ mice compared with SOD1^{G93A}/*Lgals1*$^{+/+}$ mice. Three mice were examined in each group. Error bars show the mean ± SEM. (**E**) Box plots showing the velocity distribution of each CTB-labeled vesicle (dot). The velocity distribution of CTB-labeled vesicles was significantly different between SOD1^{G93A}/*Lgals1*$^{-/-}$ and SOD1^{G93A}/*Lgals1*$^{+/+}$ mice ($n \geqq 155$ vesicles from 3 mice in each group). The box indicates 25 to 75% quartiles of samples with a median line, and the vertical lines show the slowest, 10% quartile, 90% quartile, 97.5% quartile and fastest vesicle in each sample, starting at the left. $^{**}P < 0.0001$, Steel-Dwass test. (**F**) The average velocity of CTB-labeled vesicles in each mouse was not significantly different between SOD1^{G93A}/*Lgals1*$^{+/+}$ and SOD1^{G93A} /*Lgals1*$^{-/-}$ mice ($n = 3$ mice in each group). Error bars show the mean ± SEM. $^{*}P < 0.05$, $^{**}P < 0.01$, one-way ANOVA ($P = 0.0059$) followed by individual post hoc Tukey's HSD test. Scale bars, 500 μm (**A**), 50 μm (**B**), 100 sec (**C**, y axis), 5 μm (**C**, x axis).

Supporting information

Additional Supporting Information may be found in the online version of this article:

Figure S1. Measurements of the internal diameters of axons. The shortest side of a box (dashed line) surrounding an axon was measured as the internal diameter of the axon (arrow). Scale bars, 1 μm.

Figure S2. Low-power field view of double immunofluorescence staining of the lumbar cord with anti-neurofilament and anti-rhGAL-1 antibodies. In SOD1^{G93A}/*Lgals1*$^{+/+}$ mice, large aggregates with neurofilament IR (green, arrows) were often observed especially at the anterior root exit zone, and which were mostly galectin-1 IR positive (red). In SOD1^{G93A}/*Lgals1*$^{-/-}$ mice, aggregates with neurofilament IR were also found (dashed arrows) with no galectin-1 IR, but their sizes were clearly decreased compared with SOD1^{G93A}/*Lgals1*$^{+/+}$ mice. Cell nuclei were counter-stained with DAPI (blue). Scale bars, 100 μm.

Figure S3. Quantitative western blotting of galectin-1 in extracts prepared from whole spinal cord. Two additional sets of data for Figure 4**C** obtained from wild-type (WT) and SOD1^{G93A}/*Lgals1*$^{+/+}$ (SOD) mice as shown in Figure 4**B** are presented.

Figure S4. Kaplan-Meire graphs showing the onset of rotarod failure. (**A**) and 10% body weight loss (**B**). There was no statistically significant difference between SOD1^{G93A}/*Lgals1*$^{+/+}$ mice (n = 11) and SOD1^{G93A}/*Lgals1*$^{-/-}$ mice (n = 11) in the onset of

rotarod failure (P = 0.5451, log-rank test) and 10% body weight loss (P = 0.8201, log-rank test).

Figure S5. Electron microscopy of myelinated axons in the lumbar cord. An additional three sets of images from the electron microscopy data shown in Figure 6**B** are presented. Swollen axons (≧ 4 μm) were marked with an asterisk. Black asterisks show axons containing vacuoles and white asterisks show axons without vacuoles. The diameters of swollen axons in SOD1^{G93A}/*Lgals1*$^{-/-}$ mice were smaller than those in SOD1^{G93A}/*Lgals1*$^{+/+}$ mice and accumulation of vacuoles was less frequently observed in SOD1^{G93A}/*Lgals1*$^{-/-}$ mice, even in swollen axons. Scale bars, 5 μm.

Figure S6. Frequency distribution of axon diameters. Relative frequency (%) of axons with given diameter in wild-type, SOD1^{G93A}/*Lgals1*$^{+/+}$, and SOD1^{G93A}/*Lgals1*$^{-/-}$ mice are shown in bar graphs. In SOD1^{G93A}/*Lgals1*$^{+/+}$ and SOD1^{G93A}/*Lgals1*$^{-/-}$ mice, the relative frequencies of axons containing vacuoles are shown by dark bars. In SOD1^{G93A}/*Lgals1*$^{+/+}$ mice, axons with an internal diameter larger than 4 μm were increased and most of those contained vacuoles. In SOD1^{G93A}/*Lgals1*$^{-/-}$ mice, large swollen axons were less frequently observed and the proportion of axons containing vacuoles was lower compared with SOD1^{G93A}/*Lgals1*$^{+/+}$ mice. Three mice were examined in each group, and the total numbers of axons examined were 318 axons in wild-type, 911 axons in SOD1^{G93A}/*Lgals1*$^{+/+}$, and 1071 axons in SOD1^{G93A}/*Lgals1*$^{-/-}$. Error bars show the mean ± SEM.

Video S1. Time-lapse imaging of CTB-labeled vesicles in isolated sciatic nerve from wild-type mice at 28 weeks of age. Images recorded for 174.4 s are shown.

Video S2. Time-lapse imaging of CTB-labeled vesicles in isolated sciatic nerve from $SOD1^{G93A}$/*Lgals1*$^{+/+}$ mice at 28 weeks of age. Images recorded for 174.4 s are shown.

Video S3. Time-lapse imaging of CTB-labeled vesicles in isolated sciatic nerve from $SOD1^{G93A}$ /*Lgals1*$^{-/-}$ mice at 28 weeks of age. Images recorded for 174.4 s are shown.

Figure 1

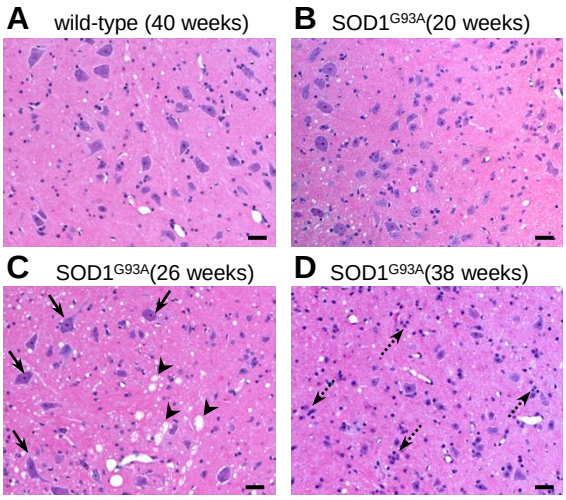
A wild-type (40 weeks)
B SOD1G93A(20 weeks)
C SOD1G93A(26 weeks)
D SOD1G93A(38 weeks)

Figure 2

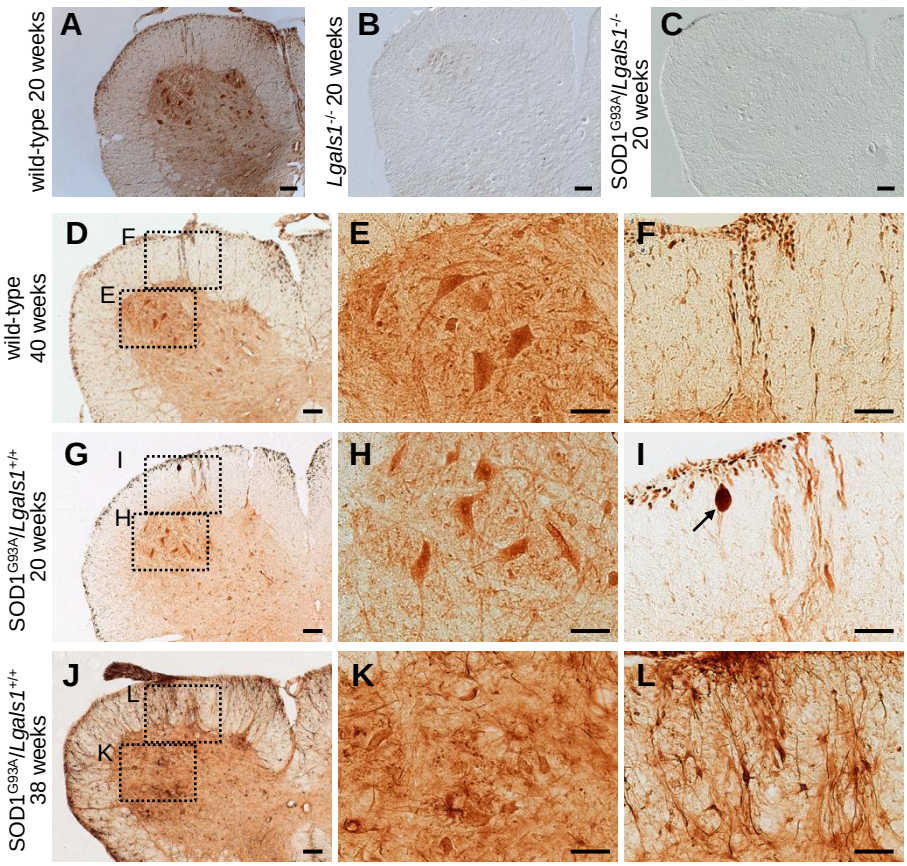
wild-type 20 weeks
A
Lgals1-/- 20 weeks
B
SOD1G93A/Lgals1-/-
20 weeks
C
wild-type
40 weeks
D
F
E
E
F
SOD1G93A/Lgals1+/+
20 weeks
G
I
H
H
I
SOD1G93A/Lgals1+/+
38 weeks
J
L
K
K
L

Figure 3

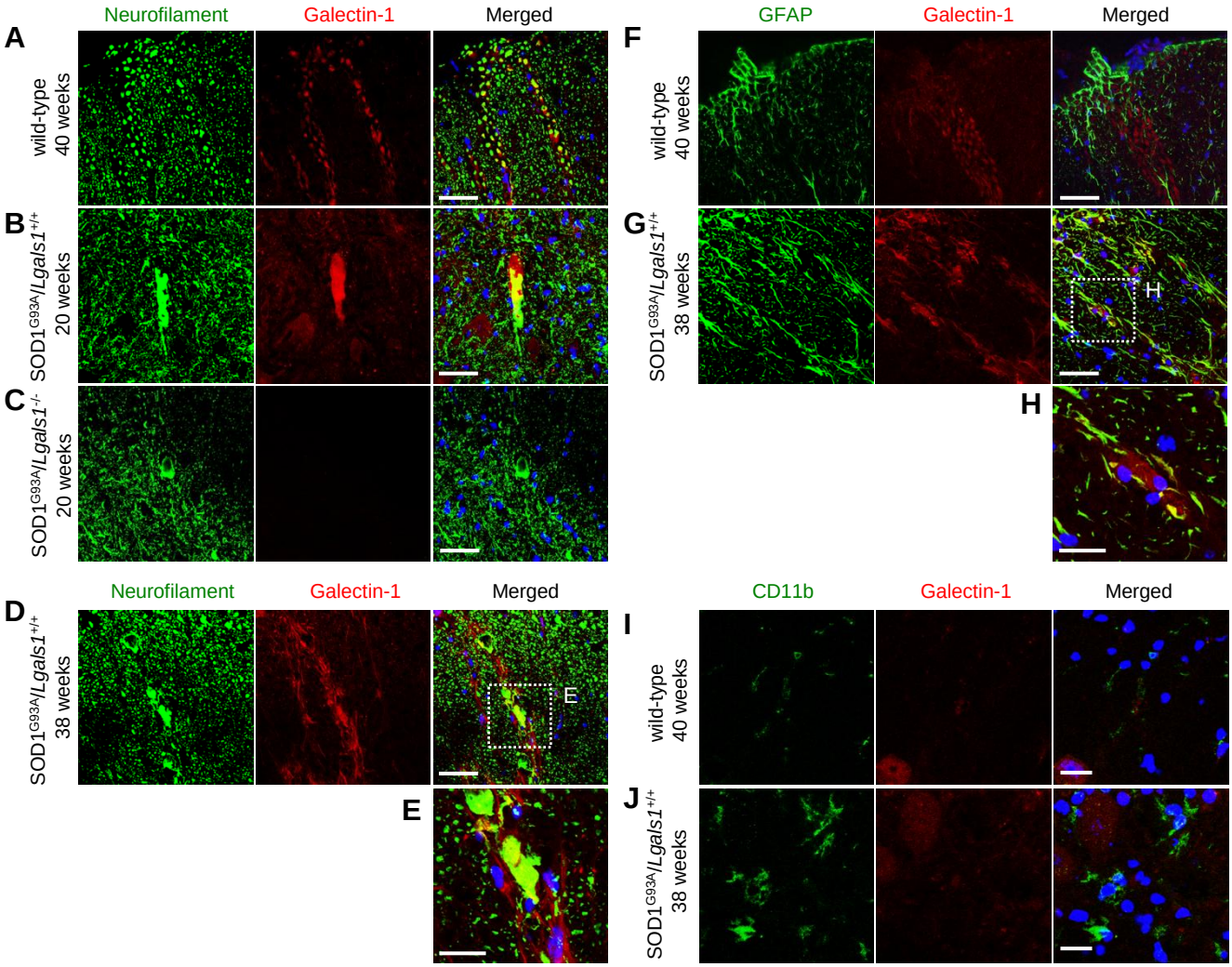
Neurofilament
Galectin-1
Merged
A
wild-type 40 weeks
B
SOD1G93A/Lgals1+/+ 20 weeks
C
SOD1G93A/Lgals1-/- 20 weeks
GFAP
Galectin-1
Merged
F
wild-type 40 weeks
G
SOD1G93A/Lgals1+/+ 38 weeks
H
H
Neurofilament
Galectin-1
Merged
D
SOD1G93A/Lgals1+/+ 38 weeks
E
E
CD11b
Galectin-1
Merged
I
wild-type 40 weeks
J
SOD1G93A/Lgals1+/+ 38 weeks

Figure 4

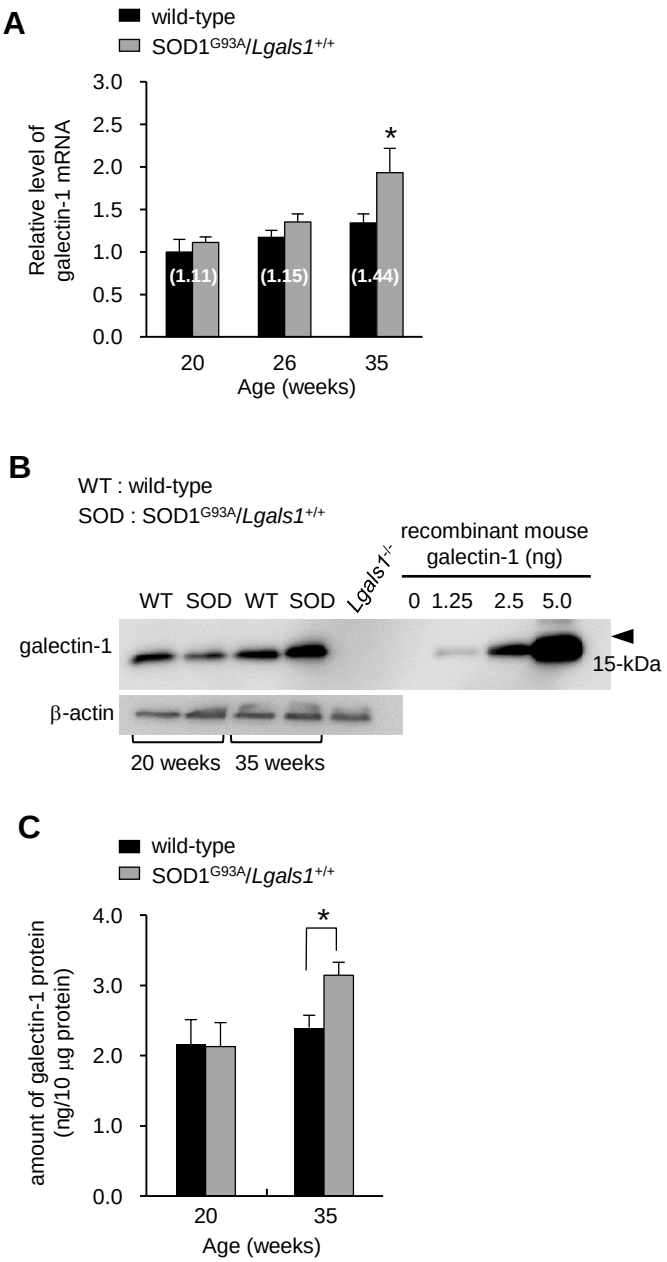
A
wild-type
SOD1G93A/Lgals1+/+
Relative level of galectin-1 mRNA
3.0
2.5
2.0
1.5
1.0
0.5
0.0
*
(1.11)
(1.15)
(1.44)
20
26
35
Age (weeks)
B
WT : wild-type
SOD : SOD1G93A/Lgals1+/+
recombinant mouse galectin-1 (ng)
WT SOD WT SOD Lgals1-/- 0 1.25 2.5 5.0
galectin-1
15-kDa
β-actin
20 weeks 35 weeks
C
wild-type
SOD1G93A/Lgals1+/+
amount of galectin-1 protein (ng/10 μg protein)
4.0
3.0
2.0
1.0
0.0
*
20
35
Age (weeks)

Figure 5

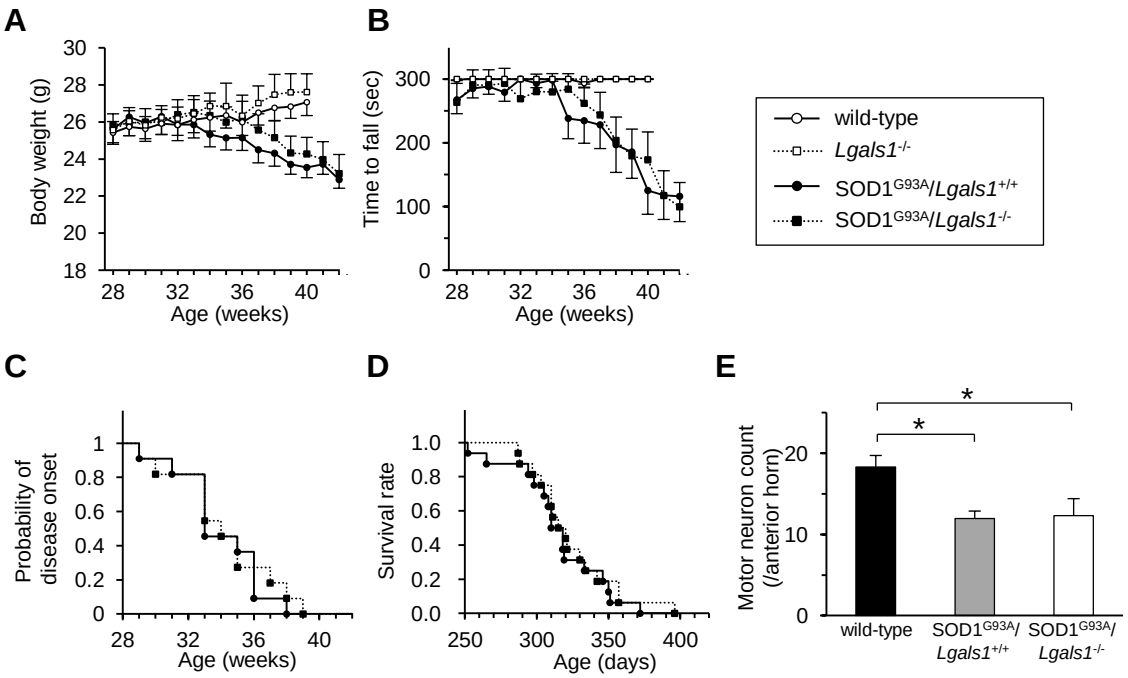
A
Body weight (g)
30
28
26
24
22
20
18
28
32
36
40
Age (weeks)
B
Time to fall (sec)
300
200
100
0
28
32
36
40
Age (weeks)
wild-type
Lgals1-/-
SOD1G93A/Lgals1+/+
SOD1G93A/Lgals1-/-
C
Probability of disease onset
1
0.8
0.6
0.4
0.2
0
28
32
36
40
Age (weeks)
D
Survival rate
1.0
0.8
0.6
0.4
0.2
0.0
250
300
350
400
Age (days)
E
Motor neuron count (/anterior horn)
20
10
0
*
*
wild-type
SOD1G93A/ Lgals1+/+
SOD1G93A/ Lgals1-/-

Figure 6

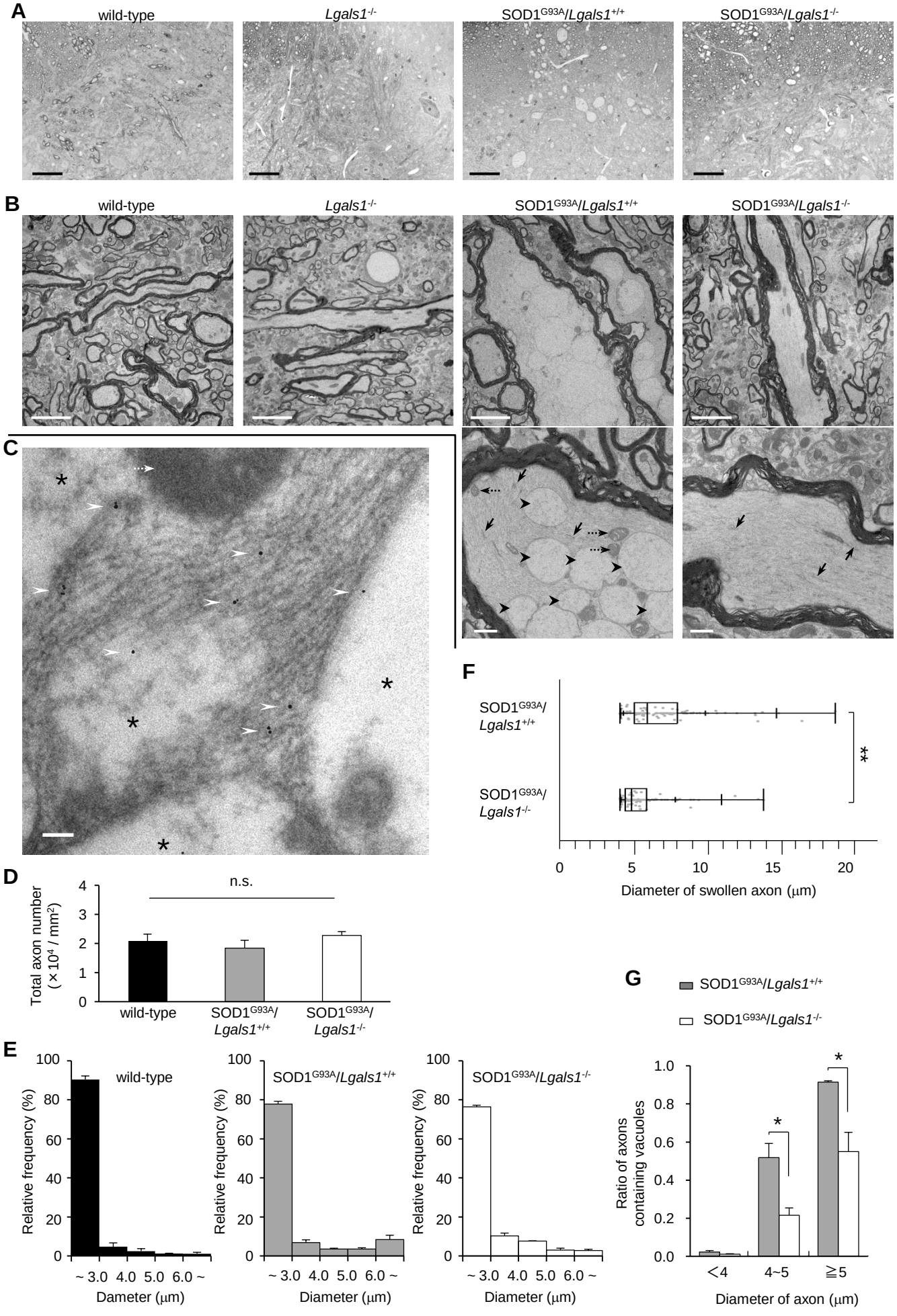
A
wild-type
Lgals1-/-
SOD1G93A/Lgals1+/+
SOD1G93A/Lgals1-/-
B
wild-type
Lgals1-/-
SOD1G93A/Lgals1+/+
SOD1G93A/Lgals1-/-
C
D
n.s.
Total axon number (×10⁴ / mm²)
wild-type
SOD1G93A/ Lgals1+/+
SOD1G93A/ Lgals1-/-
E
wild-type
SOD1G93A/Lgals1+/+
SOD1G93A/Lgals1-/-
Relative frequency (%)
~ 3.0 4.0 5.0 6.0 ~
Diameter (μm)
F
SOD1G93A/ Lgals1+/+
SOD1G93A/ Lgals1-/-
**
Diameter of swollen axon (μm)
G
SOD1G93A/Lgals1+/+
SOD1G93A/Lgals1-/-
Ratio of axons containing vacuoles
<4
4~5
≧5
Diameter of axon (μm)

Figure 7

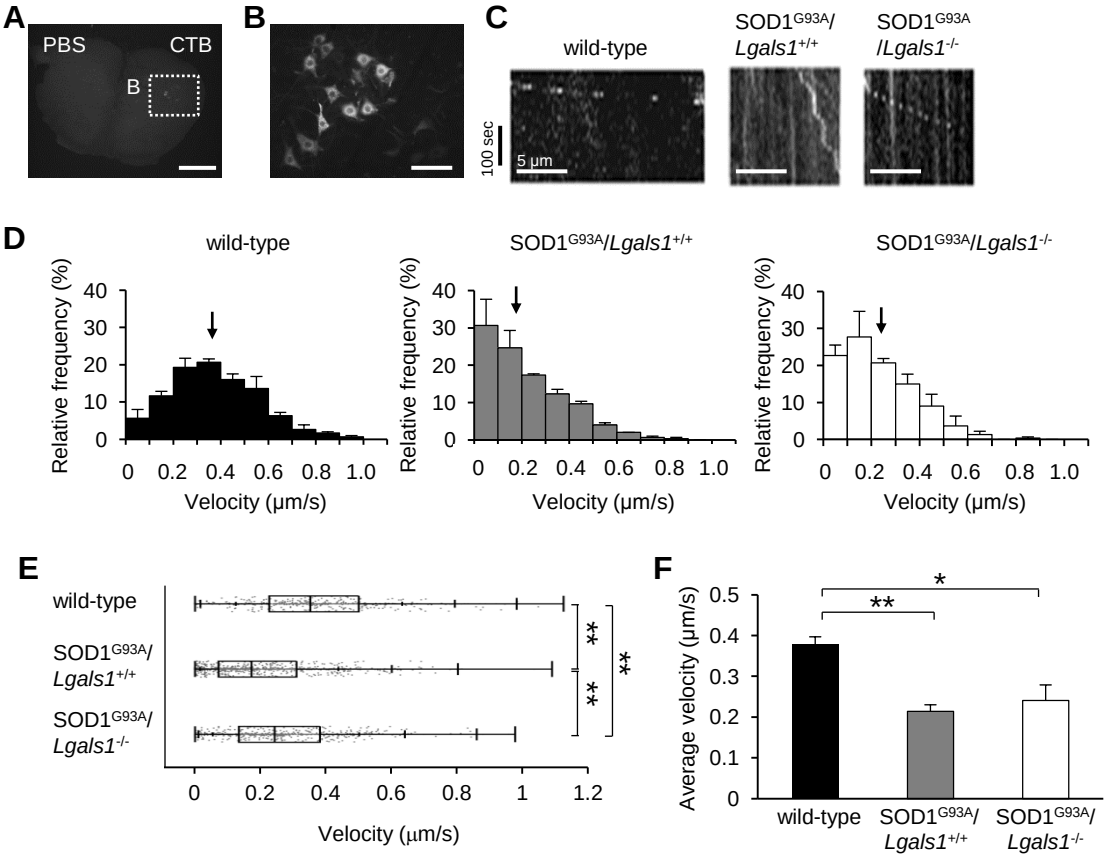
A
PBS
CTB
B
B
C
wild-type
SOD1G93A/
Lgals1+/+
SOD1G93A
/Lgals1-/-
100 sec
5 μm
D
wild-type
SOD1G93A/Lgals1+/+
SOD1G93A/Lgals1-/-
Relative frequency (%)
Velocity (μm/s)
E
wild-type
SOD1G93A/
Lgals1+/+
SOD1G93A/
Lgals1-/-
**
**
**
Velocity (μm/s)
F
Average velocity (μm/s)
*
**
wild-type
SOD1G93A/
Lgals1+/+
SOD1G93A/
Lgals1-/-